TOPICAL REVIEW

Micromachined high-g accelerometers: a review

V Narasimhan[1], **H Li**[2†], **M Jianmin**[2]

[1] Temasek Laboratories @ NTU, Division of Microsystems, Research Techno Plaza, BorderX Block, 50 Nanyang Drive, 8th Storey, Singapore 637553
[2] School of Mechanical & Aerospace Engineering, Nanyang Technological University, 50 Nanyang Avenue, Singapore 639798

E-mail: HoldenLi@ntu.edu.sg

Abstract. This paper reviews research and commercial development of high-g micromachined accelerometers. Emphasis is given on different high-g sensing schemes and popular design templates used to achieve high-g sensing. Additionally, trends in high-g micromachined accelerometer development both in research and in the market are discussed.

Submitted to: *J. Micromech. Microeng.*

1. Introduction

Today, micromachined inertial sensors, primarily accelerometers, are one of the most important types of silicon-based technologies. Microaccelerometers alone have the second largest sales volume after pressure sensors [1, 2]. Accelerometers are extensively used in numerous industries such as automotive, biomedical, consumer electronics, robotics and military [1, 3]. However, more research and commercial emphasis has been given towards the low-g measuring range, thus making high-g sensing a niche field [4].

The last two decades have witnessed an ever-increasing involvement in this sector of accelerometer development in order to meet highly specific needs such as structural destruction, rupture and collision process, munition and fuze applications, etc. [5–12]. Table 1 provides a summary of common applications of micromachined accelerometers based on g-range.

This paper presents a critical review of high-g micromachined accelerometers summarizing popular research and commercial developments. Furthermore, trends in high-g sensing are also covered. Finally, despite the plethora of work realised in this field over the past few decades, no documentation of this progress has been made within the research community. Therefore, this paper aims to provide researchers

† Author to whom any correspondence should be addressed.

Table 1. Common applications of micromachined accelerometers based on g-range.

G-range (g)	Common applications
<10	Consumer applications [1,3,13,14]
<100	Car airbag [15–17]
<1,000	Crash testing [18]
10,000–30,000	Structural destruction, munition, fuze, blast testing, pyroshock [5–12,19]

with a guide to gain a better understanding of all research and commercial developments in the field of high-g shock sensing in order to aid their research.

Generally, all micromachined accelerometer structures are modelled after the conventional spring-mass-damper system as shown in figure 1. They consist of a proof mass m that is suspended by complaint beams or flexures of spring constant k anchored to a fixed frame. Additionally, there is a viscous damping factor b impacting the movement of the mass. External acceleration displaces the proof mass relative to the fixed frame, which in turn stresses the flexures. By employing this physical phenomenon, several sensing schemes can be used to determine the external acceleration. The transfer function in 1 below can be used to mathematically map the aforementioned relationship [1],

$$H(s) = \frac{x(s)}{a(s)} = (s^2 + \frac{bs}{m} + \frac{k}{m})^{-1} = (s^2 + \frac{\omega_r}{Q} + \omega_r^2)^{-1} \tag{1}$$

Here, x is the displacement of the proof mass and a is the external acceleration. The resonance frequency of the structure is given by $\omega_r = \sqrt{k/m}$ and the quality factor of the system is $Q = m\omega_r/b$.

The sensitivity of the accelerometer can be mathematically described as in 2,

$$\frac{x}{a} = \frac{m}{k} = \frac{1}{\omega_r} \tag{2}$$

It is evident that in order to measure large shock accelerations, a wide frequency bandwidth is required to protect the sensor from resonance [9, 10]. Therefore a structural solution to the problem would be to increase the stiffness of the structure while reducing the mass of the proof mass [1].

Considering accelerometers in general, piezoresistive and capacitive transduction are the most prominent sensing schemes used in commercial devices [3]. The development of bulk micromachining and wafer bonding techniques saw a rise in piezoresistive accelerometer development towards low-g applications [1, 13]. These devices either used a bonded three-wafer system (glass caping with a silicon middle-wafer) [13] or a lower glass base and a silicon overhang serving as a shock stop and for damping [20, 21]. In the case of capacitive accelerometers used extensively for low-g applications, vertical and lateral structures have been the most widely demonstrated [1]. In vertical structures, the proof mass is separated by a narrow air gap

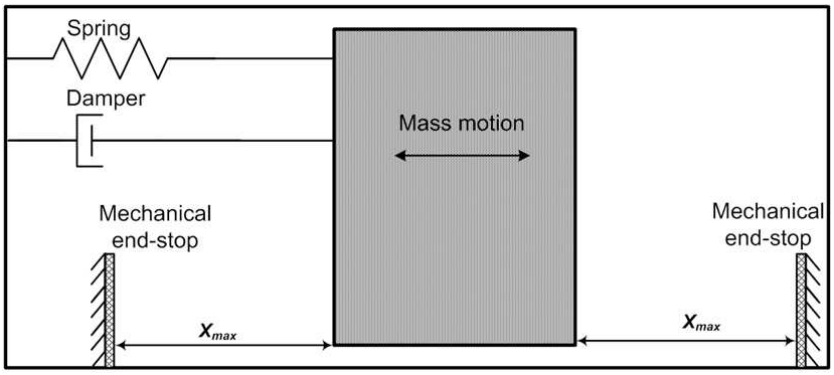

Figure 1. An accelerometer modelled after a spring-mass-damper system. For high-g accelerometers especially, end stops are designed to ensure high shock survivability [3].

from a fixed electrode forming a parallel plate capacitor. The movement of the proof mass in the z-axis when acted upon by an external acceleration varies this air gap and therefore the capacitance [22–24]. Such early designs used bulk micromachined techniques and wafer bonding to achieve large volume proof masses and high sensitivities [22, 24]. With the advent of surface micromaching, lateral structures with interdigitated finger like comb drive capacitors were developed [25, 26].

For high-g sensing in particular, piezoresistive and piezoelectric sensing dominate the market as well as research [19]. A consideration in high-g design is survivability. Low-g designs as described earlier cannot simply be scaled to meet high-g requirements owing to this consideration. In fact, even many commercially available legacy accelerometers for impact sensing are primarily for one-time use due to their tendency to resonate at high frequency environments [27]. This proves to be the root cause for many problems in high-g shock measurement [19]. Current solutions to the problem include mechanical or electrical filtering and high structural resonance [19]. Promising approaches so far have been in-built mechanical filtering as achieved by Sandia National Laboratories for example [19,28] and studies conducted on over-range capacity through mechanical stops [29–31] or through structural damping [27,32]. However, these approaches increase the size of the device preventing it from being used in certain applications that require small size [27]. Despite such advancements, the measurement of true-impulses in extremely harsh enviroments such as in pyroshock testing for example remains to be adequately addressed. Currently, near-true impulses still affect high-g accelerometers causing sensor failure and non-repeatability. The scope of this paper will be limited to popular high-g piezoresistive and piezoelectric sensing schemes as well as sensor trends which have aimed to address these issues over the years.

2. Popular high-g accelerometer sensing schemes

Conventionally, a variety of transduction mechanisms are used for microaccelerometer sensing. However, as mentioned in section 1, the two most popular approaches for high-g shock sensing are piezoresistive and piezoelectric sensing.

2.1. Piezoresistive sensors

The piezoresistive effect is characterized the change in electrical resistivity of a semiconductor or metal when acted upon by a mechanical strain. This phenomenon was first observed by Lord Kelvin in metals [33]. Usually, the resistance change in metals occurs due to geometrical changes resulting from applied mechanical strains. In conducting and semi-conducting materials, mechanical strains tend to alter the inter-atomic spacing thereby affecting the bandgaps. This makes it easier (or harder depending on the material and strain) for electrons to be raised into the conduction band thus resulting in a change in resistivity of the material. Within a certain range of strain this relationship has been varified to be linear. Even though the piezoresistive effect is small in metals, in most cases the phenomenon is not negligible. It is computed through the familiar resistance equation derived from Ohm's law. In the case of semiconductors like silicon however, the piezoresistive effect is several orders of magnitude higher than the geometrical effect. The effect of piezoresistivity in semiconductors can further be amplified by doping them with impurity charge carriers. This enables the development of highly sensitive doped silicon-based piezoresistive sensing gauges.

Microsensor development today has been rapidly revolutionized by the extensive use of silicon micromachining which leverages the unique properties of silicon [4, 34]. One such property is that of piezoresistance. The main advantages of piezoresistive accelerometers are the simplicity of their structures and the fabrication process used to manufacture them, as well as the readout circuitry since the Wheatstone bridge generates a low output-impedance DC voltage [1, 5].

Single crystal silicon is known to have a diamond lattice crystal structure. Early work from Smith [35], and Kanda and co-workers [36–39] characterizing large piezoresistive coefficients in silicon paved the way for its extensive use as a piezoresistor. Smith [35] applied the Bridgman tensor notation [40] in defining the piezoresistive coefficients and geometry of his test configurations. He went on to determine the piezoresistive coefficients for relatively lightly doped silicon and germanium $\left(100\right)$ samples along the $\left[100\right]$ and $\left[110\right]$ directions with resistivities ranging from 1.5 to 22.7 Ω-cm [3, 35]. Current commercial and research practices however use higher dopant concentrations [3].

The first fully functional micromachined piezoresistive accelerometer was developed by Roylance and Angell in 1978 for biomedical applications [13, 14]. Their cantilever-lumped mass based approach is still widely adopted today. However,

as such conventional methods have reached their limits, recent developments in micromachining techniques have opened up the possibility of realizing far more complex structures meeting specific requirements such as high-g applications [8].

Often used in weaponry, piezoresistive high-g micromachined accelerometers are of great significance in national defence [6]. For such applications, these sensors would need to work under high impact conditions ranging between 100,000 and 200,000 g [6, 41, 42]. However, owing to the highly proprietary nature of such technology, there are few public reports and engineering applications about the high-g accelerometers. Also, such accelerometers are expensive and very difficult to procure as sale is often strictly controlled by international arms regulatory bodies [6].

Ning et al. developed one of the first high-g piezoresistive MEMS accelerometer with a performance range of up to 100,000 g [4]. The device adopted a cantilever beam approach without a lumped mass in order to obtain a large working bandwidth of over 100 kHz. Figure 2 illustrates the dimensions (in μm) of the structure along with the piezoresistors present at the top.

Rapidly evolving microfabrication techniques such as Deep Reactive Ion Etching (DRIE) and Silicon On Insulator (SOI) to name a few, have resulted in the development of microstructures that were inconceivable in the past [5, 6, 9, 10, 31, 43].

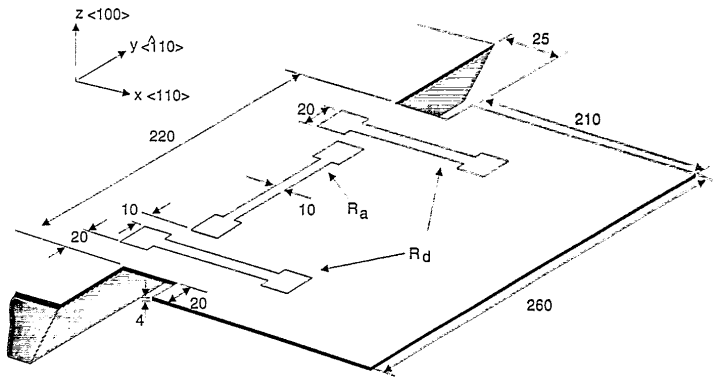

Figure 2. A cantilever-based high-g accelerometer without a proof mass [4]. R_a and R_d represent the transverse and longitudinal piezoresistor arrangement used. All dimensions are in μm.

2.1.1. Popular structures

(i) **Twin-mass-plate structure**

Owing to the simplicity of the fabrication techniques used to realize piezoresistive transducers, some popular structures have been developed and utilized extensively through the years. A twin-mass-plate structure first thoroughly analyzed by Shen et al. in 1992 [44] was utilized effectively by Wang et al. [11] and Dong et al. [5] more than a decade later. The structure consists of two proof masses instead of one and five flexures instead of two or four as

Table 2. The sensitivity and natural frequency of the twin-mass accelerometer for different plate thicknesses [11].

Plate thickness (μm)	Sensitivity ($\mu V/V/g$)	Natural frequency (kHz)
30	8.1	72
80	1.10	277
100	0.74	353
120	0.48	431

seen on old cantilever-based designs [44]. The completely uniform and single sign (either tensile or compressive) nature of the stresses on the central beam makes it an ideal location for the sensing elements.The twin-mass-plate structure is a successor of the conventional cantilever [45, 46] and a two or four beam (quad beam) structure [47, 48]. It offers a more optimized normal sensitivity–bandwidth product as opposed to its two predecessors. Furthermore, its lateral sensitivity readout is far less. Figure 3 shows a schematic of the twin-mass structure presented by both Shen et al. [44] and Wang et al. [11]. The stated sensitivity of this structure is governed by the structural design according to the following equation [49]:

$$S = \frac{3\rho h_2 a_2 (a_2 + 2a_1)(1 - \nu^2)}{4h_1^2} V_{\text{supply}} \pi_{44} \tag{3}$$

Here, ρ is the density of silicon while π_{44} and ν are its piezoresistive coefficient and Poisson's ratio respectively. V_{supply} is the voltage in volts. The dimensions of the structure are defined by a_1, a_2, h_1 and h_2 (see figure 3). Table 2 shows the performance characteristics of the twin-mass-plate structure as per simulations [11].

There are two main advantages of this structure. First, the fabrication process is extremely simple and the structure is easily scalable to different g ranges as shown in Table 2. Secondly, the four piezoresistors as shown in figure 3 are oriented such that two are located on the side plates and the other two are on the central plate indicating that all four composing the Wheatstone bridge are subjected to transverse stresses reducing non-linearity and lateral effects [49,50]. However, as observed by 3, the sensitivity is dependent upon a_1, a_2 and h_1. These variables must be controlled extremely accurately through a design process that includes the use of Silicon On Insulator (SOI) technology. This poses to be one of the potential limitations of the twin-mass-plate structure as it relies upon expensive manufacturing processes thus hindering the possibility of mass production.

The twin-mass-plate structures have been achieved via wafer bonding as well. These bonded structures have been developed to serve as accelerometers for high-g applications. Fan et al. arrived at a two-wafer bonded hinge structure

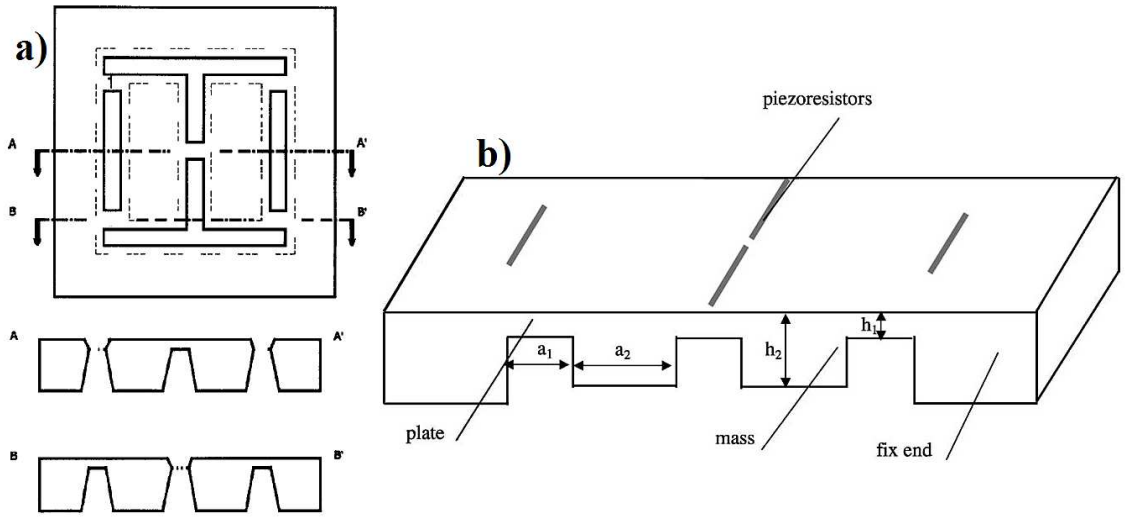

Figure 3. Twin-mass-plate structure as illustrated by a) Shen et al. without DRIE [44]. and b) Wang et al. with DRIE [11]. Sensing axis is perpendicular to the wafer plane.

wherein the proof mass is held in place by two hinges with sensing beams located on both sides [10]. Four resistors on the top surface along the sensing beams form a full bridge. Figure 4 presents a schematic of the set-up indicating the two different substrates used to fabricate the sense beams and the support hinges respectively. The figure also shows a CCD micrograph of the fabricated chip.

This approach provides advantages such as allowing for individual optimization of the different functioning parts of the sensor, in this case the sense and the support beams. However, bonded structures pose a host of design and fabrication related challenges. First, even small bonding misalignments can be detrimental to performance at high-g ranges [51]. Further, processes such as bonding require the wafer surface to be extremely clean, flat and polished. Any surface roughness or dirt can lead to unbonded areas also known as voids where interface bubbles can occur [52]. Owing to such apparent shortcomings, this approach is not widely adopted.

(ii) **Cantilever structure**

Following the work done by Ning et al. [4], several groups still adopt this conventional approach despite contention regarding its use for high-g applications. This is owing to its susceptibility to large lateral or cross-axis effects and fragility leading to poor yield during mass production [44]. As mentioned in section 2.1, to meet such rigorous requirements, most cantilever structures do not assume a lumped-mass approach in order to boost the operational bandwidth. Dong et al. developed a cantilever-based accelerometer for lateral shock measurement [31]. Two identical cantilevers are laid out antagonistically in order to form a full Wheatstone bridge as demonstrated earlier by Partridge

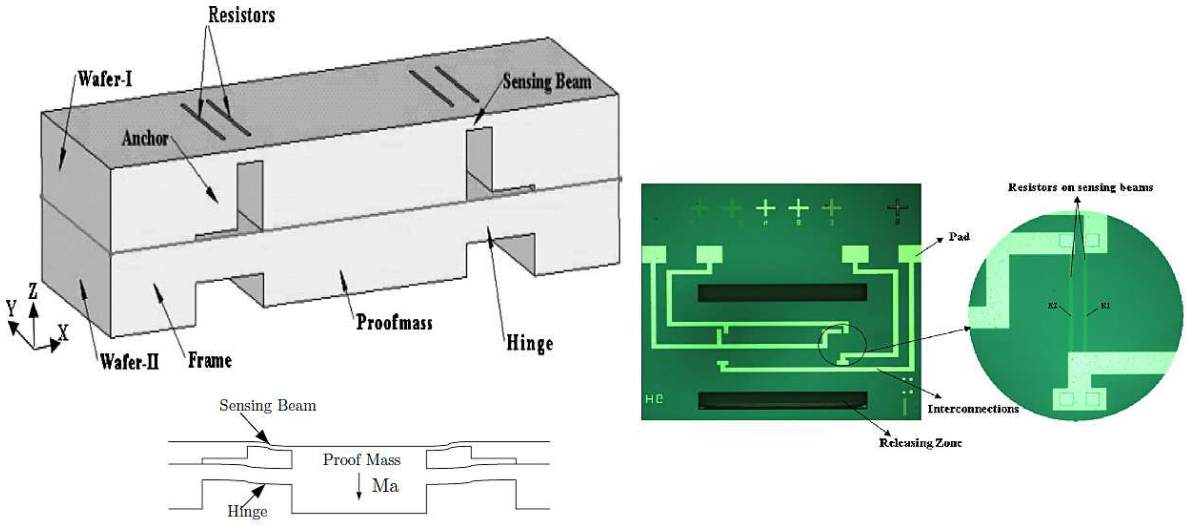

Figure 4. Schematic of the bonded structure indicating two different wafer substrates for sensing and support as well as a CCD micrograph of the chip and resistors [10].Sensing axis is perpendicular to the wafer plane.

et al. [53] for low-g applications. As per literature, the theoretical sensitivity of this structure can be expressed as per 4 [31],

$$S = \frac{3\pi_{44} V_{\text{supply}} h' \rho (l - L)^2}{h^2} \tag{4}$$

where h' is the distance between the resistor and the neutral plane of the cantilever, l is the distance between the base of the cantilever and the center of the resistor, and L and h are the length and thickness respectively.

Dong et al. in their work highlighted the need for efficient over-range stop structures for shock survival in high-g environments [31]. Until then, a single-point stop structure was used for high-g accelerometers [54, 55]. However if the cantilever has to deflect under an over-range shock, its movement can be checked far better using a curved surface. This provides an ever-point stop application method that offers better protection at high-g ranges [55]. Figure 5 illustrates the design of Dong et al. [31].

Wang et al. [9] arrived at a dual-cantilever that addressed a common fabrication problem experienced while realizing most cantilever-based accelerometers [4,31, 53]. Most cantilever structures reported prior to Wang et al. [9] were fabricated with KOH etching from the bottom to thin the silicon wafer at the cantilever location with an additional DRIE step for release. However, the KOH etching step is often slow and cannot be controlled accurately when fabricating small structures. In order to solve this fabrication issue, Wang et al. proposed a single-sided fabrication on a (111) silicon wafer based on the study of its crystallographic and piezoresistive properties [56, 57]. Designed to measure lateral shock, two identical devices are placed in parallel to form a full bridge.

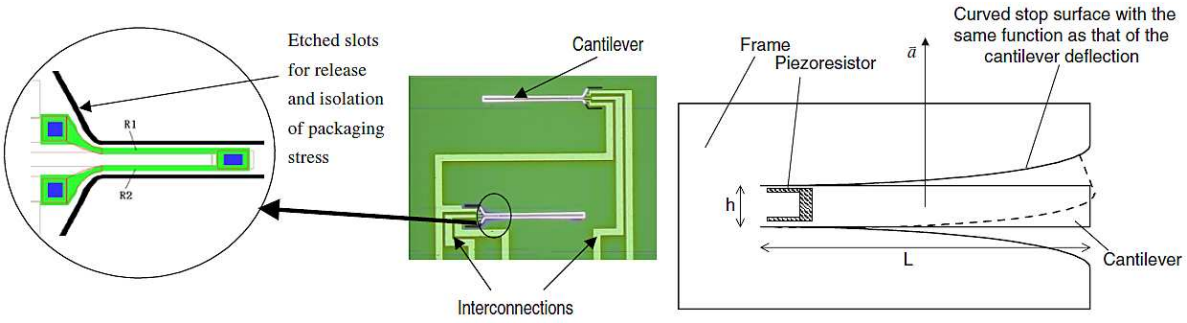

Figure 5. Design of Dong et al. presenting a CCD micrograph of the fabricated sensor chip consisting of two indentical cantilevers laid out oppositely. A schematic of the curved stop surface is also displayed [31]. Sensing axis is as indicated by $\bar{a}$.

The theoretical sensitivity of the structure is shown in 5 [9]:

$$S = \frac{\pi_{44} V_{\text{supply}} h' \rho (l^2 - 3lL + 3L^2)}{h^2} \tag{5}$$

where all notations are as per 4.

From the work of Dong et al. [31] and Wang et al. [9], it is apparent that the current cantilever accelerometer design trend is to adopt a lateral sensing cantilever without a proof mass such that the aspect ratio of the cantilever cross-section is designed to decrease the cross-axis sensitivity. However, the approach is restricted by process limitations such as the maximum attainable aspect ratio. When the gaps between the lateral cantilevers and the side stops are in the order of a few microns, it becomes fairly difficult to maintain a consistent profile through the bulk of the wafer. This would in turn affect the profile of the cantilever and impact sensor performance.

More recently Zhao et al. used the SOI technique to achieve a tighter control on cantilever dimensions [6]. This cantilever is used to sense out-of-plane accelerations normal to the device surface. The SOI material can withstand high temperature which plays an integral part in high-g sensing.

(iii) **Tiny beam structure**

The tiny beam structure was first reported by Suminto from the company Endevco sensing systems for the 7264B series of accelerometers [28, 30]. The sensor was designed on a (110) silicon wafer utilizing the anisotropic nature of etching along the [111] direction, which forms the vertical walls [30]. This shock accelerometer demonstrated survivability beyond the 10,000 g range and consisted of three layers – two protective caps and an active movable core layer. The resistors were tiny beams placed within the core layer such that the sensing axis lies along the plane of the sensor rather than perpendicular to it. Furthermore, the resistors are designed to be very short and at a precise distance from the central supporting hinge so that even extremely small displacements produce large axial stresses.

After Suminto, Huang et al. developed a piezoresistive accelerometer consisting of two axially stressed tiny beams that work in tandem with a central supporting cantilever beam [43]. Having a very fine cross-section, these tiny beams act as stress concentrators and are therefore optimal locations for resistor placement. This approach provides high sensitivity and a broader bandwidth as it is very scalable to different g-ranges. Various sensors using the same platform were designed and simulated to measure ranges from 0.25 g to 25000 g [43]. The tiny beam structure was developed keeping in mind the drawbacks of conventional cantilever accelerometers such as a low sensitivity–bandwidth product and its inability to meet high-g applications [5, 18, 43, 44]. Tiny beam accelerometers can be classified broadly into two categories a) a purely axial deformation scheme [5, 18, 30, 43] and b) an axial plus bending deformation scheme [58–60]. The purely axial deformation scheme is obtained by optimizing geometric parameters such as the distance between the tiny beam and the central supporting cantilever as in the case of Huang et al [43]. It is claimed that this method provides a highly uniform stress pattern leading to a uniform output from the varistor. In order to attain precision over the thickness of the tiny beam, SOI wafers are used as they are crucial to attain a uniform axial stress. Figure 6 shows a schematic of the work done by Huang et al. as well as SEM images of the device. However Huang et al. only presented a fabricated device with a measuring range of 2 g in their work [43]. The extension of their design to high-g ranges is only justified through simulation.

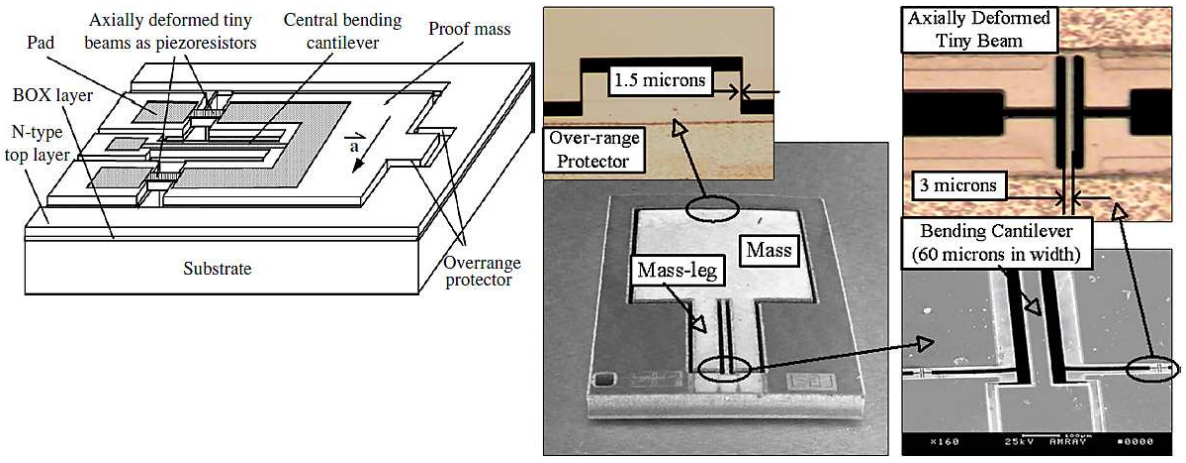

Figure 6. Schematic of the accelerometer developed by Huang et al. as well as SEM images of the same [43]. The fabricated device is however only capable of measuring up to 2 g. Sensing axis is as indicated by $\vec{a}$.

As seen in figure 6, the system consists of a central bending cantilever supporting a large proof mass flanked by two tiny beam piezoresistors on either end. The tiny beams are placed at an optimal distance from the central cantilever so as to be deformed purely axially when the device deflects laterally under an applied

acceleration. The sensitivity of this tiny beam set-up is provided in 6 [43],

$$S = \frac{\sqrt{6}\pi_{44} V_{\text{supply}} \rho L^2 \sqrt{TK}}{48\sqrt{bhl}} \tag{6}$$

where L is the length of the central cantilever, T is the bulk thickness, K is a design parameter dependent upon the size of the individual components of the device and their relative positions, while b, h and l are the width, thickness and length of the tiny beams respectively.

Dong et al. used a very similar approach to arrive at an axial tiny beam crash accelerometer [18]. However, this design was fabricated and characterized at 2000 g thus serving as a proof of concept theorized by earlier work in a high-g environment [18]. Further, Dong et al. designed a novel comb damper system to increase the resonance frequency of the structure and act as a multi-point stopper in order to meet high-g requirements [18].

Kuells et al. designed and fabricated a piezoresistive shock accelerometer structure using a tiny beam axial and bending deformation concept [59]. A schematic along with an optical image of the sensor is shown in figure 7. This sensor follows the axial and bending deformation scheme since the gauges bend under downward acceleration onto the flexural plate to which they were connected.

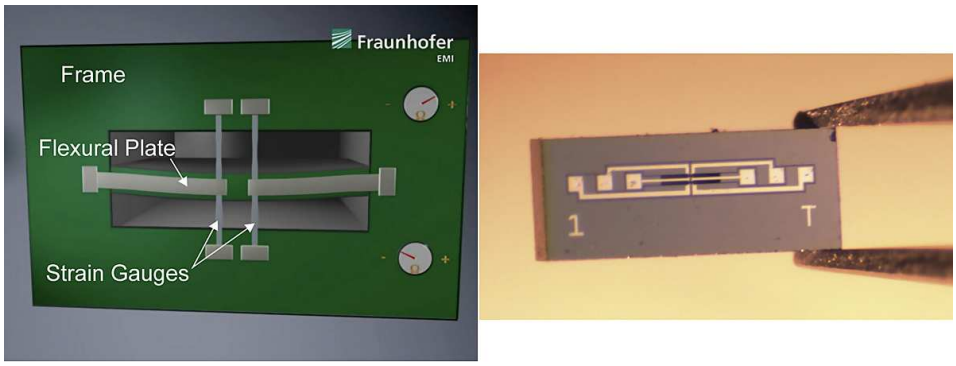

Figure 7. 3D illustration of the device developed by Kuells et al. displaying piezoresistive elements spanning the trenches that define the central flexural plate and a photograph of the sensor chip [59]. Sensing axis is perpendicular to the wafer plane.

A major drawback of the tiny beam structure is its susceptibility to cross-axis loading. In the case of axial planar tiny beams as in Huang et al., the reported cross-axis sensitivity in the normal direction is about 7.3%, which is fairly high given current standards [43]. Furthermore, to obtain a purely axial stress on the tiny beam is rather difficult, as there is always the likelihood of an infusion of stress due to bending given the slender nature of the piezoresistors. Therefore despite being highly sensitive when compared to the twin-mass-plate structure, the tiny beam is prone to coupling effects. However, very recently, work by

Wung et al. has demonstrated negligible cross-axis effects as low as 0.21% on a tiny beam based high-g microaccelerometer when tested on a rate table upto 3000 g [61].

(iv) **Triaxial structures**

In the first three categories of micromachined piezoresistive accelerometers, only single-axis sensors have been developed. Triaxial strctures form an important category under structural design as several design requirements need to be met in order to conceptualize them. Triaxial accelerometers are often needed for the simultaneous detection of all three principle components of the acceleration vector. These structures can be classified into three primary categories a)those employing a single proof mass, b) three individual elements mounted together in a single package and c) monolithically fabricated and isolated elements. The first category consisting of single proof mass accelerometers have been researched extensively [7, 8, 62–65] and patented [66–72]. This scheme consists of a proof mass used to track accelerations on all three primary axes and is supported by flexures, thus forming a simple spring-mass-damper system. Despite offering advantages such as a simplified construction and small bulk plus overall package size, the single seismic mass accelerometers have a major drawback. This lies in their susceptibility to strong cross-axis coupling due to the use of a single seismic mass [5, 73]. These designs show large disparities in performance parameters such as frequency response or resolution across different axes as they utilize three different bending modes of the same spring-mass system to respond to all acceleration inputs [74]. For example, in the case of Lin et al., the stated sensitivity of the sensor along the x and y axes is 0.37 μV/V/g whereas the sensitivity along the z axis is 2.1 μV/V/g leading to a huge performance disparity.

The second category is constructed by simply mounting three single axis devices in a single package. Many inertial measurement units (IMUs) consist of an integration of commercial off-the-shelf (COTS) single-axis sensors. While this method is adopted as a quick solution potentially saving on development time to manufacture traditional triaxial accelerometers, the cost of procuring single-axis sensors and integrating them is usually high. Furthermore, this approach cannot be translated into mass production.

The third category is the most novel and promising approach to triaxial high-g sensing. Studies have reported monolithically integrated triaxial accelerometers consisting of three or more independent sensing elements for both high-g [5, 73] using piezoresistive sensing and low-g using capacitive sensing schemes [74, 75]. These accelerometers use one specific type of element for the purpose of sensing accelerations parallel to the chip plane and another type for sensing perpendicular to the chip plane. Due to the inherent planarity of the fabrication processes, it is hard to get the same properties, bandwidth and resolution for the two different types of sensing elements [11]. One of the pioneering

works in integrated triaxial accelerometers through independent elements was demonstrated by Matsumoto et al. [75]. Despite attaining good sensitivity as well as handling fabrication issues such as stiction which is commonly experienced during the HF solution release process, the device was characterized to have a cross-axis sensitivity of under 10% which is still fairly erroneous. Even in the case of Rödjegård et al. [74], despite using a novel four-proof mass design, based on reported sensitivities, it is seen that the cross axis effects along the horizontal and vertical were roughly 9% and 14% respectively.

Dong et al. [5, 73] ingeniously developed a monolithically fabricated triaxial accelerometer consisting of three isolated sensing elements. The x and y axis elements utilized followed the tiny beam structure reported by Huang et al. [43] and the z axis element drew influence from the twin-mass-plate structure reported by Wang et al. [11]. Figure 8 presents a schematic as well as SEM images of the structure [5, 73]. The theoretical sensitivity of the structure follows those reported by Huang et al. [43] and Wang et al. [11] in 3 and 6.

Dong et al. reported cross-axis sensitivities under 2.1% [5]. However, with resonant frequencies of 308, 303 and 164 kHz for the x, y and z sensing elements respectively, there is a fair amount of disparity in performance parameters as generally witnessed in single proof mass triaxial sensors. The three elements could have been better tuned to match the performance of one another. Furthermore, based on the device linearity plot, up to 20,000 g, a fair amount of amplification is needed for the readout.

This again highlights the issue of non-uniform performance between the individual sensing elements due to the inherent planarity that is obtained through monolithic fabrication.

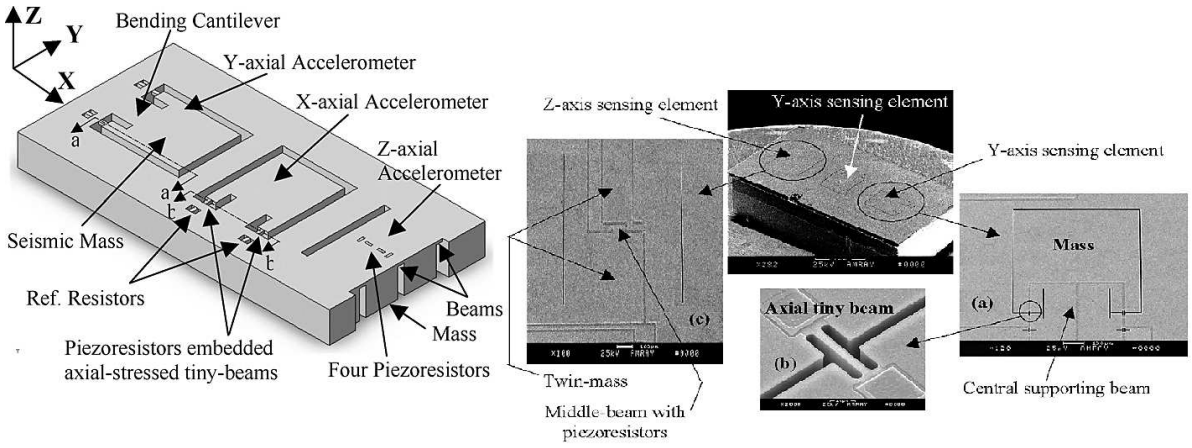

Figure 8. Schematic and SEM images of a monolithically integrated triaxial accelerometer with sensing elements adopted from prior work [5, 11, 43]. Sensing axis is as indicated on the schematic.

(v) **Other structural approaches**

Over the years the use of silicon carbide (SiC) has garnered considerable attention as a potential material to replace silicon in micromachined sensors [76]. Researchers at NASA, the US Air Force Research Laboratory and Cornell University have proposed the use of an alternate material namely 6H-SiC, to the more conventionally adopted silicon in the development of high-g accelerometers [77,78]. This is owing to the fact that material properties of silicon may not allow for reliable operation in high temperature environments unless more robust and expensive packaging methods are used [78, 79]. SiC also has a higher Young's modulus of 448 GPa [80] as opposed to silicon's 129 GPa in the $\left(100\right)$ plane [81]. Furthermore, SiC is not susceptible to thermally induced plastic deformation as is silicon in excess of 500 ^{o}C and also has a higher bandgap than single crystal silicon [77,78].

A multi-axis single seismic mass high-g accelerometer was developed by Atwell et al. [77] and Okojie et al [78]. based on the 6H-SiC material platform. Four prototypes were presented, all of which adopted a diaphragm-boss structure. Figure 9 illustrates the schematics of the four structures as well as an SEM image of the fourth structure.

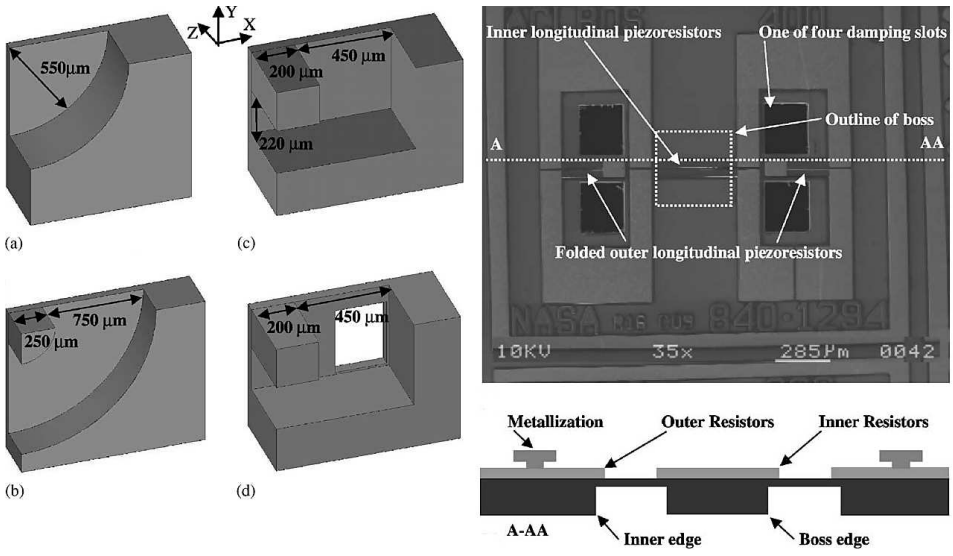

Figure 9. Schematic sections of four structures labelled (a)-(d) along with an SEM image with a cross-section illustration of structure [77, 78]. Sensing axis is perpendicular to the wafer plane.

Despite the novelty of this approach as well as the emergence of SiC as a potential alternative to silicon in micromachined accelerometer design, several drawbacks exist. First, SiC has a relatively low gauge factor of 30 [82] compared to that of silicon which is about 90 [83]. This limits its use as a piezoresistive sensor as it would heavily impact the device sensitivity. Secondly, the commercial applications of such accelerometers are seriously restricted by the expenses and manufacturing challenges of using 6H-SiC [10].

2.1.2. Piezoresistive sensor trends

Two important parameters – sensitivity and bandwidth – characterize the overall performance of a high-g accelerometer and therefore form the foundation for design optimization.

Sensitivity of an accelerometer is defined as the measurement signal (conventionally in volts) per unit acceleration experienced by the sensor. Bandwidth is given by the mechanical resonant frequency of the device structure [59]. These two parameters are related to each another by the following relationship that has been widely used in research [1,43,59]:

$$\phi = S\omega_o^2 \tag{7}$$

here, ω_o denotes the lowest resonant frequency or the first mode of the mechanical structure and S denotes its sensitivity. The variable ϕ depends on the measurement method as well as the overall geometry of the system under consideration. It is evident that an increase in the sensitivity and the bandwidth simultaneously can be achieved through maximizing ϕ. However, a common problem faced in the design process is that sensitivity and bandwidth vary antagonistically making this optimization hard to achieve. ϕ in turn provides a gauge to compare the design characteristics of one accelerometer with another and is therefore termed as a figure of merit for benchmarking high-g micromachined accelerometers.

Table 3 summarizes the aforementioned concept and compares some of the currently available high-g piezoresisitive MEMS accelerometers fabricated commercially or demonstrated in research.

Though the sensitivity–bandwidth product constant serves as an important figure of merit, it is not the sole criterion used in determining the quality of an accelerometer. Cross-axis sensitivity, damping, manufacturability, etc. are other important gauges used [59]. A drawback of this analysis is that this figure of merit can be increased upon increase in device resonant frequency since ϕ varies with square of ω_o [59]. This would drastically lower device sensitivity within the input ranges of interest. This figure of merit should be viewed as a measure of an accelerometer's performance within acceptable bounds for resonant frequency. Therefore, this gauge is useful when comparing devices structured around similar magnitudes of resonant frequencies and dynamic ranges.

To further analyse trends in both commercial and researched high-g piezoresistive accelerometers, a variance of resonant mode and sensitivity with dynamic range of various sensors is presented in figure 10. Figure 11 presents a plot that captures the dependence of dynamic response on resonant mode of various commercial accelerometers. A practical limitation is evident in this analysis which caps the maximum sensitivity and dynamic response frequency as well as the minimum resonant mode achievable for a given dynamic range. This limit is arrived at empirically.

Table 3. A list of high-g piezoresistive accelerometers and their figures of merit.

Research group / Model no.	Structure type	Dynamic range (kg)	Sensitivity ($\mu V/V/g$)	Natural fre-quency (kHz)	Figure of merit ($(\phi) \times 10^5$)
			Research		
[11]	Twin-mass-plate	20	1.43	220	0.69
[10]	Twin-mass-plate - bonded	200	0.516	573	1.69
[31]	Cantilever	100	3	83.6	0.21
[9]	Cantilever	200	0.71	79	0.04
[6]	Cantilever	50	5.4	213.53	2.46
[4]	Cantilever	100	0.72	107	0.082
[18]	Tiny beam - axial	2	110	31	1.06
[61]	Tiny beam - axial	10	3	232.40	1.62
[59]	Tiny beam - axial+bending	200	D_1=0.13 D_2=0.035 D_3=0.23 †	3350 3680 2670	14.59 4.74 16.4
[7]	Triaxial - single proof mass	200	D_z=2.1 D_x=D_y=0.37 †	236	1.17 0.21
[63]	Triaxial - single proof mass	200	D_x=D_y=0.45 D_z=0.6	503.75 311.98	1.14 0.58
[5,73]	Triaxial - isolated sensing elements	100	D_x=2.17 D_y=2.25 D_z=2.64	308 303 164	2.06 2.07 0.71
[77,78]	Alternate methods - SiC	100	D_1=0.05 D_2=0.125 D_3=0.213	875 657 253	0.38 0.54 0.14
			Commercial		
PCB 3501 Series [84]					
A202KG	—	2	20	20	0.08
A2020KG	—	20	1	60	0.04

Research group/ Model no.	Structure type	Dynamic range (kg)	Sensitivity ($\mu V/V/g$)	Natural fre- -quency (kHz)	Figure of merit ($(\phi) \times 10^5$)
A1220KG	—	20	1	60	0.04
A2060KG	—	60	0.3	120	0.04
Endevco Series [28]					
71-6K	—	6	30	20	0.12
71-20K	—	20	10	50	0.25
71-60K	—	60	3	100	0.3
727-2K	—	2	10	10	0.01
727-6K	—	6	3	20	0.01
727-20K	—	20	1	50	0.03
727-60K	—	60	0.3	100	0.03
7270A-2K	—	2	100	90	8.1
7270A-6K	—	6	30	180	9.72
7270A-20K	—	20	10	350	12.25
7270A-60K	—	60	3	700	14.7
7270A-200K	—	200	1	1200	14.4

Another metric worth considering for characterizing the performance of any accelerometer including those performing at high-g spectra is accelerometer noise. For a variety of reasons discussed in previous sections, the need to scale down acclerometer devices has always shown promise. For example, as mentioned earlier, in order to measure large shock accelerations, structural alterations such as increase of stiffness and reducing the mass of the proof mass would be required [1, 9, 10]. However, this leaves out a very important consideration - the smaller the devices are, the lower is the Signal-to-Noise Ratio (SNR) [85, 86]. A mathematical definition

† D_1, D_2 and D_3 are the sensitivities of three different devices developed. D_z, D_x and D_y are the sensitivities along the z, x and y axes respectively.

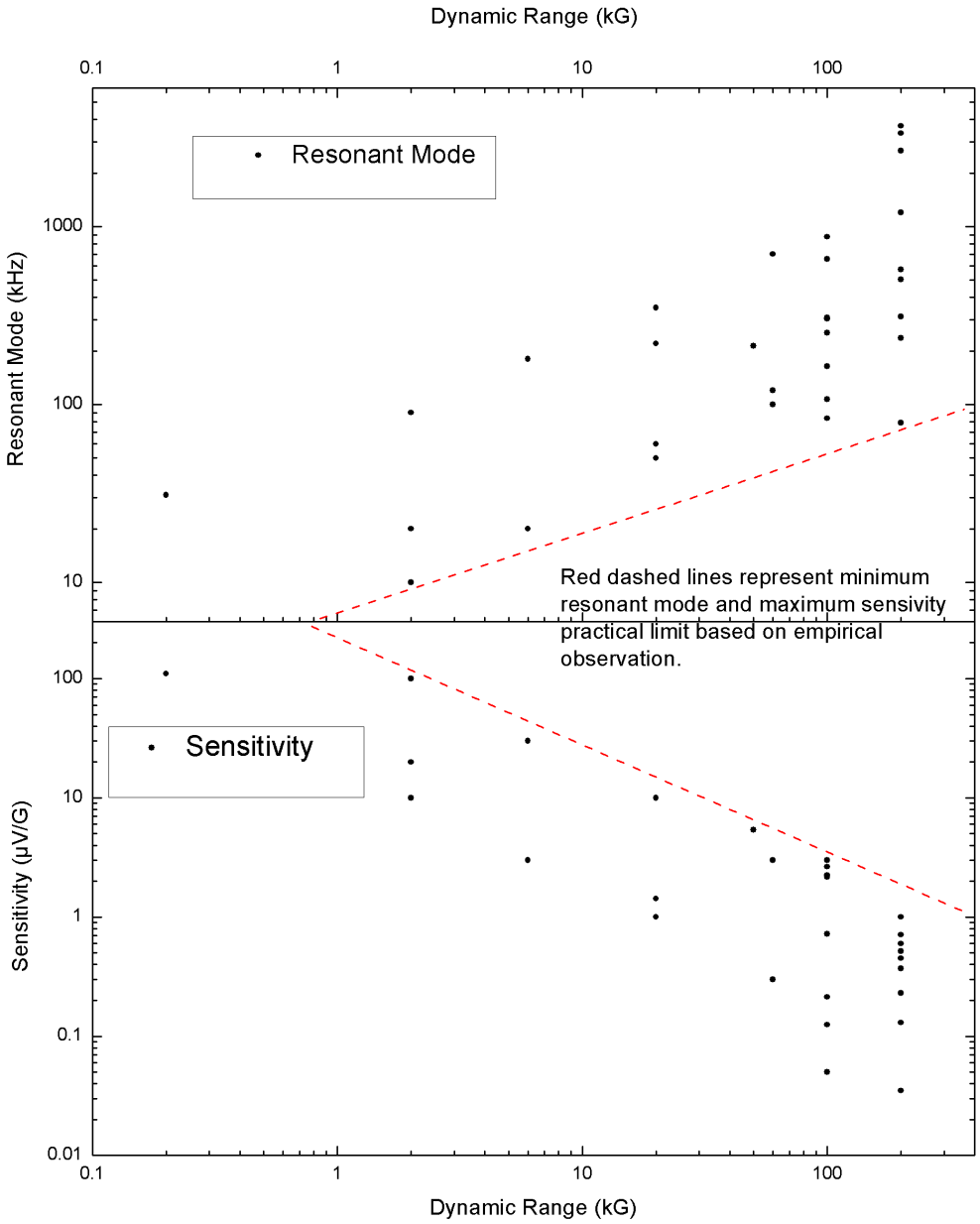

Figure 10. Plot of the variance of resonant mode and sensitivity of various high-g piezoresistive accelerometers with their dynamic range. The practical limitation is bounded by red dashed lines. Units for dynamic range expressed in *kG* (or *kg* in some cases).

of accelerometer RMS noise density is given below [87]:

$$< a_n > \approx \sqrt{\frac{4kT\omega_o}{mQ}} \tag{8}$$

where k and T are the Boltzmann constant and temperature in Kelvin scale

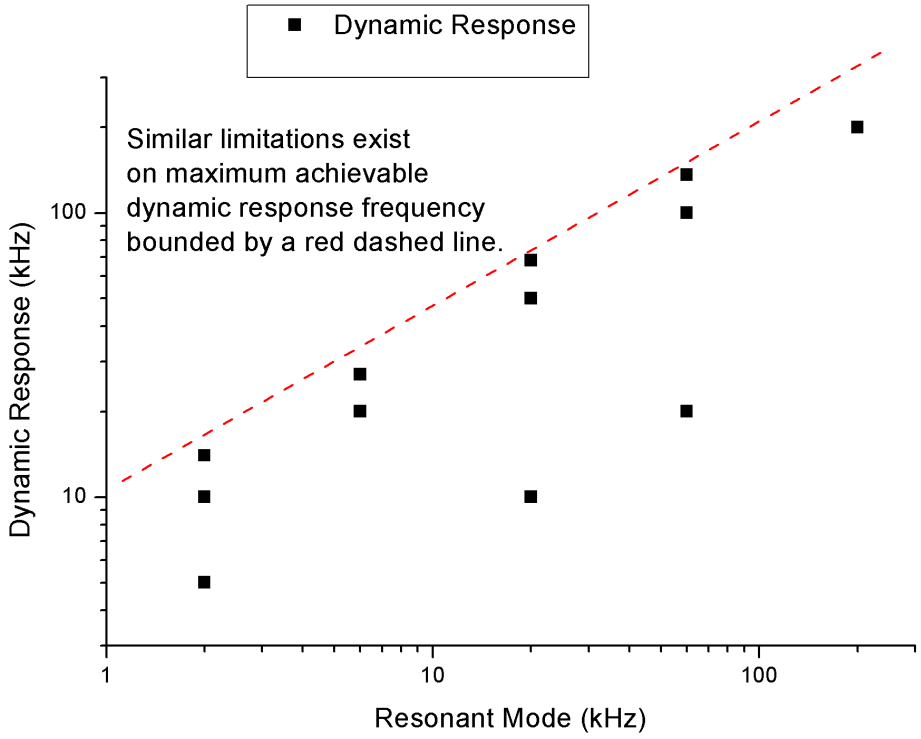

Figure 11. Plot of dynamic response vs resonant mode of various commercial high-g piezoresistive accelerometers. Similar limitation based trends are observed as with other sensor characteristics.

respectively. The terms ω_o, m and Q are terms described earlier in 1 and 7. The quality factor Q was defined in section 1 as $Q = m\omega_r/b$ with ω_r being a different representation for resonant frequency ω_o. The expression was derived from a frequency independent expression analogous to Johnson-Nyguist noise in resistors [88] and the equation of motion for the accelerometer system [87]. Here, with some simple manipulation:

$$\begin{aligned} Q &= \frac{\sqrt{km}}{b} \\ b_{cr} &= 2\sqrt{km} \\ Q &= \frac{1}{2\xi} \end{aligned} \tag{9}$$

b_{cr} is the critical damping of the system and therefore the damping ratio $\xi = b/b_{cr}$. The expression for accelerometer RMS noise density can now be expressed in terms of ξ as:

$$< a_n > \approx \sqrt{\frac{8kT\omega_o\xi}{m}} \tag{10}$$

Table 4. List of popular commercially available piezoresistive high-g micromachined accelerometers and their noise characteristics [84].

Model	Bandwidth (kHz)	Mass (g)	Damping Ratio ($\%b_{cr}$)	RMS Noise Density ($\mu g/\sqrt{Hz}$)	LSB RMS Noise (mg)
PCB 3501 Series [84]					
A202KG	20	0.15	0.7	0.17	0.02
A2020KG	60	0.15	5	0.80	0.20
A1220KG	60	2.5	5	0.20	0.05
A2060KG	120	0.15	2	0.72	0.25
A1260KG	120	2.5	2	0.18	0.06
PCB 3991 Series [84]					
A112KG	20	1.28	0.7	0.06	0.01
A1120KG	60	1.28	5	0.28	0.07
A3020KG	60	0.04	5	0.16	0.14
A1160KG	120	1.28	2	0.25	0.09
A3060KG	120	0.04	2	0.38	0.48

the above expression 10 can be used to obtain the noise as LSB RMS or Least Significant Bit Root-Mean-Square. This is a measure of the noise in terms of the smallest detectable change in acceleration in units of gs. The LSB RMS noise is taken over the bandwidth of the accelerometer and is simply obtained by:

$$< a_n >_{LSBRMS} \approx \sqrt{< a_n >^2 \omega_o} \tag{11}$$

equation 11 is a very important step in characterizing accelerometer performance as it provides an estimate of the smallest decetable change in acceleration based on RMS noise. In other words, it is a measure of resolution in terms of acceleration equivalent noise. From the expression, the dependence on bandwidth is evident.

Observing 10, it can be inferred that increasing the mass, increasing the quality factor (or lowering the damping ratio) and reducing the bandwidth would all result in an increased SNR. This directly contradicts the design ideology for high-g discussed in section 1. Generally speaking however, low-noise characteristics are not of much significance when measuring very high shock signals since maximum amplitude of the signal is of major importance [89]. Nonetheless, resolution expressed in terms of RMS noise is still an important metric to address. Table 4 presents a list of computed RMS noise density as well as LSB RMS noise for several popular piezoresistive high-g micromachined accelerometers by PCB [84]. Accelerometers developed by research groups as detailed in table 3 are not presented here due to lack of sufficient noise performance data. This again points to the earlier mentioned fact about low-noise characteristics not being an important consideration for high-g accelerometer design. From table 4, for accelerometers capable of measuring 2,000 g and above, the noise encountered is indeed rather negligible.

2.2. Piezoelectric sensors

Another widely used sensing scheme for high-g accelerometers is that of piezoelectricity [90–92]. Piezoelectricity is the phenomenon by which electric charge accumulates in certain characteristic solid materials in resonse to an applied mechanical stress. In contrast to the piezoresistive effect, the piezoelectric effect causes changes in electric potential. This effect was first observed by Jacques and Pierre Curie in 1880 [93]. The nature of piezoelectricity is very similar to the occurance of electric dipole moments in solids. As every dipole is a vector of dipole density P, so is the change of polarization P in piezoelectric solids when under mechanical strains. The polarization depends on the orientation of P within the crystal, crystal symmetry as well as on the applied strain.

The primary advantages of this mode of sensing are its usability over wide frequency ranges, excellent linearity, a self-generating nature resulting in no external power requirement, a high sensitivity to mass ratio and a wide operating temperature range [90,91]. The realization of the first piezoelectric accelerometer only came much later through Yamaguchi [94] and Kato and Nakamura [95].

Among the large number of materials that have displayed piezoelectricity, only a relatively small portion are used for transduction. Fundamentally, these piezoelectric transducers can be categorized into naturally occurring and synthetic single crystals, ceramics and thin films. Quartz, being one of the most common minerals found on earth still serves as the most popular naturally occurring single crystal material used for piezoelectric transduction. Gallium orthophosphate is a synthetic crystal derived from quartz and is also widely used. Among ceramics, lead zirconate titanate, also known as PZT, is most popular followed by zinc oxide.

Keeping in mind micromachined sensors, thin film polymers such as polyvinylidene fluoride or PVDF [96–102] and ceramics such as zinc oxide [96, 103–106], PZT [96, 107–113] and aluminum nitride [96, 114, 115] are used in MEMS and other micromachined sensors as they exhibit piezoelectricity several orders greater than that of quartz and its derivatives [90, 92]. Further, they can be deposited using common micromachining processes making them suitable for mass production [90, 96, 116–118]. Today, most piezoelectric high-g accelerometers are manufactured commercially by companies like Brüel & Kjær [119], Endevco [28], Kistler [120] and PCB [84].

2.2.1. Popular structures

A comprehensive representation of the scaling and sensitivity limits of a piezoelectric accelerometer is provided by Tadigadapa et al. [96]. Considering a simple cantilever structure, the ultimate resolution, bandwidth and maximum-g tolerance are analytically modelled. This analysis is presented in figure 12.

Several practical structures are adopted for piezoelectric accelerometer designs and are discussed in the following sections. Despite the large variety of such

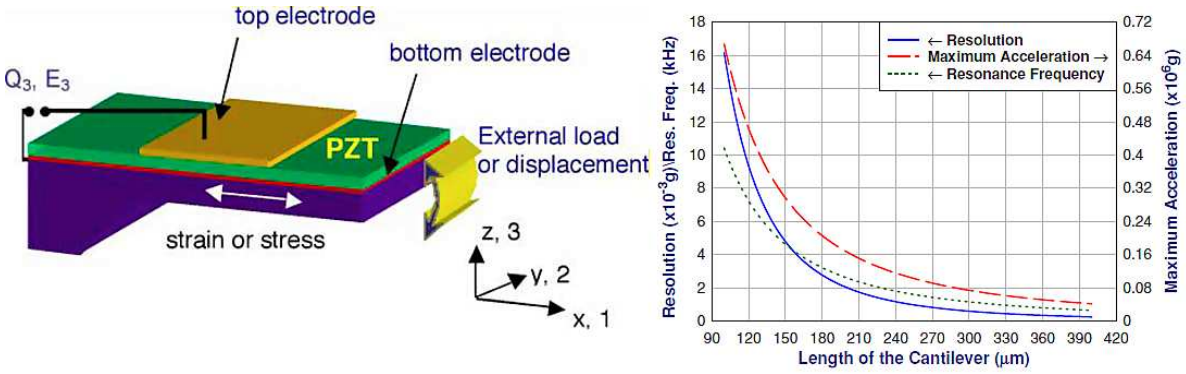

Figure 12. Simple cantilever piezoelectric accelerometer [117] and the variance of its resolution, maximum-g tolerance and resonance frequency with cantilever length [96].

accelerometers available in the market today, the design platforms adopted can be classified into one of three categories – a) shear, b) compressive and c) flexion based [90].

(i) **Shear structure**

Shear structures consist of a seismic mass which is essentially a hollow cylinder enclosing a transduction element concentrically. The transduction element is preloaded by placing a heated seismic mass on it which then cools and contracts. This ensures that there are no adhesives or bolts used to hold the assembly in place, thus providing good performance and structural reliability. Such shapes can only be designed on piezoelectric ceramics and not quartz [90]. But ceramics are pyroelectric, implying they generate charge when rapid and large temperature changes occur. This effect is highly undesirable as it affects the output from acceleration changes. However, the pyroelectric effect is exhibited only on the faces normal to the polar axis of the element. Keeping this in mind, the popularity of the shear structure has grown as more accelerometer designs exploit the shear effect on faces parallel to the polar axis where the pyroelectric effect is practically nonexistent [90]. Shear accelerometers such as the DeltaShear® by Brüel & Kjær [91, 119] and IsoShear by Endevco [28] exhibit very low temperature transient errors. Figure 13 illustrates two shear based structures developed by Brüel & Kjær – the Planar Shear and the DeltaShear® models [91, 119]. The former is a simple shear model as discussed above, while the latter consists of three radially preloaded seismic masses, each in contact with a ceramic seismic mass affixed to a triangular central stud. With relatively high sensitivity to mass ratios and bandwidths, these shear based accelerometers are primarily used for general purposes such as measuring vibrations and oscillations on machines and structures.

In recent times, designs for high-g applications are using quartz elements keeping in mind their material properties. These sensors leverage the shear

effect and have built-in charge amplifiers to provide tangible outputs. Quartz is preferred over ceramics for high-g measurements as it is usually free of zero shift, and has very high resonant frequencies and excellent inherent linearity [90,121]. Figure 14 shows one such sensor by Kistler [120].

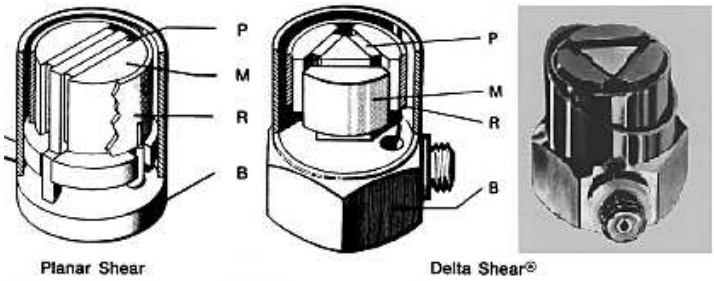

Figure 13. Planar Shear and DeltaShear® models. M-mass, P-piezoelectric element, R-clamping ring and B-base. Courtesy Brüel & Kjær [91,119].

Figure 14. Shear based high-G acclerometer. Courtesy Kistler [120].

(ii) **Compressive structure**
This structural set-up is considered the simplest of all designs. The walls of the sensor housing directly press the seismic mass against the transduction element. The two are mounted together via a centre post and a spring to a base plate forming the accelerometer [122,123]. But this arrangement is prone to dynamic changes due to bending or thermal expansions as the base and the centre post effectively behave like springs in parallel with the elements. This phenomenon causes stresses in the piezoelectric elements and therefore output errors [91,119]. Despite using thick bases, almost all compression designs are susceptible to base strain sensitivity as strain in the mounting surface is directly transferred to the transduction element.
For this reason, most compression based accelerometers are produced only for shock measurement purposes since in these regions, the output errors is insignificant when compared to the vibration signal [90,91]. Figure 15 presents a schematic of a compression based accelerometer.

(iii) **Flexion structure**
Sensors using the principle of beam bending have come into prominence owing to their low cost of manufacturing and wide use in modal analysis [90]. A

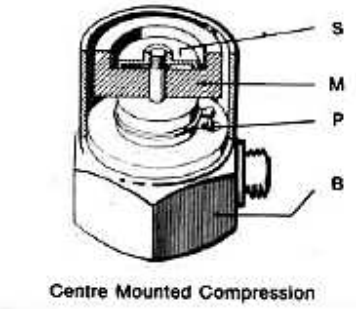

Figure 15. Schematic of compression based accelerometer. S-spring, M-mass, P-piezoelectric element, B-base. Courtesy Brüel & Kjær [91,119].

popular sensor using this design scheme is PiezoBeam® by Kistler [120]. This device uses a symmetric twin cantilever type of structure without a seismic mass. The beams are made of ceramic and are bonded together in such a way that the charge produced by the elements on the two beams will be added when subjected to acceleration. This element only reacts to normal accelerations and not angular accelerations [124,125]. Figure 16 presents a schematic of this sensor.

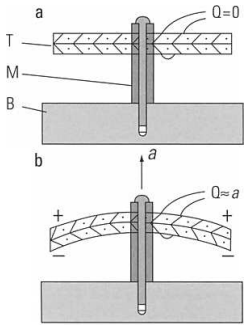

Figure 16. The PiezoBeam® design. T-beam, M-mounting post and B-base. Courtesy Kistler [120].

2.2.2. Piezoelectric sensor trends

Following commercial trends, it is observed that the largest application of piezoelectric sensors is for measuring oscillations and vibrations on machines and structures, namely general applications as mentioned earlier. The selection criteria for standard application sensors are dynamic range, sensitivity, mass, resonance frequency and operating temperature range [90]. Most sensors for the so-called general purposes category fall under the 20,000 g dynamic range. Table 5 provides an understanding of this trend. It lists almost all piezoelectric sensors available on the Endevco product catalogue [28]. From this table, it is evident that the vast majority of these sensors fall under the 20,000 g dynamic range.

While it may be desirable to procure a sensor that not only has a high dynamic range, but also a high sensitivity and low mass, there is always a trade-

Table 5. List of piezoelectric accelerometers from Endevco product catalogue. Most sensors have a measuring range of under 20 kg and are used for standard applications [28].

Endevco model	Dynamic range (kg)	Sensitivity ($\rho C/g$)	Natural frequency (kHz)
12m9	4	1.2	9
22	10	0.4	54
2220E	5	3	50
2221D	5	13.5	32
2221F	3	10	45
2222C	10	1.4	32
2222D	10	0.95	35
2223D	2	12	14
2224C	2	12	32
2225	20	0.75	100
2225M5A	100	0.25	80
2226C	2	2.8	21
2228C	2	2.8	21
2229C	2	2.8	21
2230E	2	3	21
2230EM1	2	3	21
2270	15	2.2	55
2271A	10	11.5	27
2271AM29	10	11.5	27
7201-10	20	10	48

off between the parameters as they are closely related. This has been covered in section 2.1.2 under the piezoresistive sensing scheme. The plots in figure 17 present a comprehensive overview by Gautschi of the relationship between mass, sensitivity and resonance frequency of sensors from market leaders such as Brüel & Kjær, Endevco, Kistler and PCB [90]. The sensors presented are categorized into four groups based on element material and orientation – a) quartz element for longitudinal effect, b) quartz element for transverse effect, c) ceramic element for longitudinal effect and d) ceramic element for transverse effect. Some of the general observations made were first, the mass of quartz sensors can be as high as 100 times the mass of ceramic sensors for a given sensitivity. Secondly, quartz sensors always have a slightly lower frequency than ceramic sensors for a given sensitivity. Thirdly, sensors with ultra-high bandwidth (around 250 kHz) have ceramic elements [90]. Again, as seen in the plot mapping a relationship between resonant frequency and sensor sensitivity, a clear trade-off is observed as the two parameters vary antagonistically to each other.

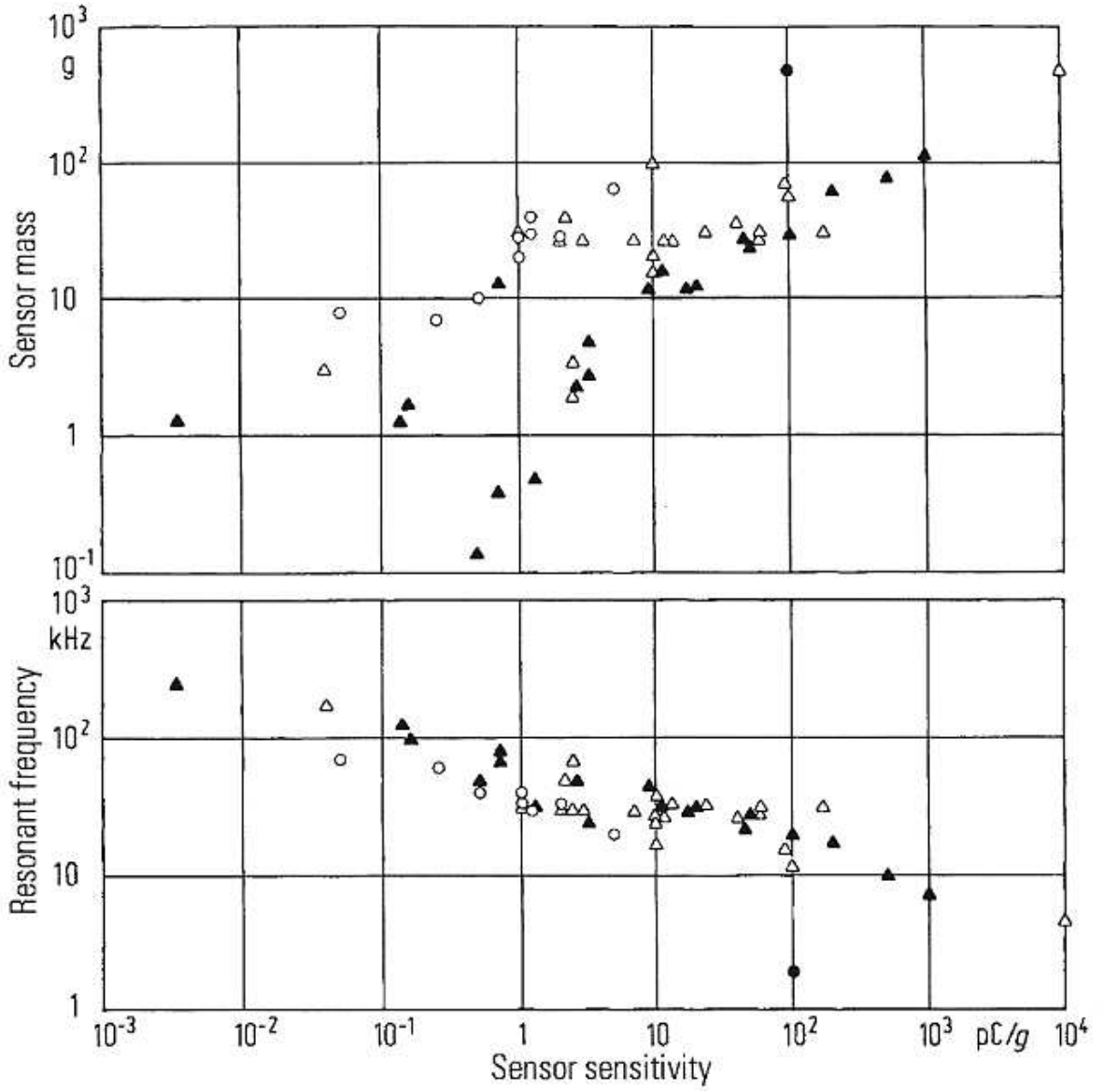

Figure 17. Plot of relationship between mass (in grams), resonance frequency (in kHz) and sensitivity (in $\rho C/g$) for various ceramic and quartz sensors from Brüel & Kjær, Endevco, Kistler and PCB. Symbols represent - quartz element for longitudinal effect (○), quartz element for transverse effect (●), ceramic element for longitudinal effect (△) and ceramic element for transverse effect (▲) [90].

Conclusion

In summary, this paper attempts to capture current innovations and issues predominating the field of high-g micromachined accelerometers by discussing design and sensing schemes as well as popular high-g sensor trends. Being a niche and lucrative sector of micromachined sensor development, design and structural advancements supported by modern approaches to fabrication of high-g micromachined accelerometers will result in greater accuracy of measurement of

shock phenomena in the future.

References

[1] Yazdi N, Ayazi F and Najafi K 1998 Micromachined inertial sensors *Proc. of the IEEE* **86** 1640

[2] Mounier E 2008 *Yole Development Report.*

[3] Barlian A A, Woo-T P, Mallon J R, Rastegar A J and Pruitt B L 2009 Review: semiconductor piezoresistance for microsystems *Proc. of the IEEE* **97** 513

[4] Ning Y, Loke Y and Mckinnon G 1995 Fabrication and characterization of high-g force, silicon piezoresistive accelerometers *Sensors Actuators A* **48** 55

[5] Dong P, Li X, Yang H, Bao H, Zhou W, Li S and Feng S 2008 High-performance monolithic triaxial piezoresistive shock accelerometers *Sensors Actuators A* **141** 339

[6] Zhao Y, Li X, Liang J and Jiang Z 2013 Design, fabrication and experiment of a MEMS piezoresistive high-g accelerometer *J. of Mechanical Science and Technology* **27** 831

[7] Lin L, Pan F, Xu J and Guo H 2010 Design of a three-axis high-g piezoresistive accelerometer *5th IEEE Int. Conf. on Nano/Micro Engineered and Molecular Systems* 773

[8] Liu L, Zhau H, Li W and Guo H 2011 Structure design and optimization of high-g piezoresistive accelerometer *Int. Conf. on Electronic and Mechanical Engineering and Information Technology (EMEIT)* 4508

[9] Wang J and Li X 2010 A high-performance dual-cantilever high-shock accelerometer single-sided micromachined in (111) silicon wafers *J. Microelectromech. Syst.* **19** 1515

[10] Fan K, Che L, Xiong B and Wang Y 2007 A silicon micromachined high-shock accelerometer with a bonded hinge structure *J. Micromech. Microeng.* **17** 1206

[11] Wang Z, Dong Z, Lu D, Xiong B, Li X and Wang Y 2003 A silicon micromachined shock accelerometer with twin-mass-plate structure *Sensors Actuators A* **107** 50

[12] Letterneau J 2012 The Endevco® high-g shock triaxial acclerometer: a smaller, more cost-effective solution to making triaxial measurements *NDIA 56th Annual Fuze Conf.*

[13] Roylance L M and Angell J 1979 Batch-fabricated silicon accelerometer *IEEE Trans. Electron Devices* **26** 1911

[14] Roylance L M 1978 A miniature integrated circuit accelerometer for biomedical applications *Ph.D., Electrical Engineering Department, Stanford University*

[15] Kim K H, Ko J S, Cho Y-H, Lee K, Kwak B M and Park K 1995 A skew-symmetric cantilever accelerometer for automotive airbag applications *Sensors Actuators A* **50** 121

[16] Zimmermann L, Ebersohl J, Hung F, Berry J P, Baillieu F, Rey P, Diem B, Renard S and Caillat P 1995 Airbag application: a microsystem including a silicon capacitive accelerometer, CMOS switched capacitor electronics and true self-test capability *Sensors Actuators A* **46** 190

[17] Zhao J, Jia J, Wang H and Li W A Novel threshold accelerometer with postbuckling structures for airbag restraint systems *IEEE Sensors* **7** 1102

[18] Dong P, Li X, Wang Y and Feng S 2006 An axial-beam piezoresistive accelerometer for high-performance crash detection of automotive industry *Sensors. Proc. of IEEE* 1481

[19] Endevco: Problems in high-shock measurement *Endevco Technical Paper 308*

[20] Barth P W, Pourahmadi F, Mayer R, Poydock J and Petersen K 1988 A monolithic silicon accelerometer with integral air damping and overrange protection *Tech. Dig. Solid-State Sensors and Actuators Workshop* 35

[21] Pourahmadi F, Christel L and Petersen K 1992 Silicon accelerometer with new thermal self-test mechanism *Tech. Dig. Solid-State Sensors and Actuators Workshop* 122

[22] Seidel H, Reidel R, Kolbeck R, Muck G, Kupke W and Koniger M 1990 Capacitive silicon accelerometer with highly symmetric design *Sensors Actuators A* **21** 312

[23] Peeters E, Vergote S, Puers B and Sansen W 1992 A highly symmetrical capacitive micro-accelerometer with single degree-of-freedom resonse *J. Micromech. Microeng.* **2** 104

[24] Rudolf F, Jornod A, Berqovist J and Leuthold H 1990 Precision accelerometers with μg resolution *Sensors Actuators A* **21** 297
[25] Boser B and Howe R T 1996 Surface micromachined accelerometers *J. Solid-State Circuits* **31** 366
[26] Chau K, Lewis S R, Zhao Y, Howe R T, Bart S F and Marcheselli R G 1995 An integrated force-balanced capacitve accelerometer for low-g applications *Tech. Dig. 8th Int. Conf. on Solid-State Sensors and Actuators (Transducers95)* 593
[27] Endevco: Survivability and linearity of the high-survivability, high-shock 60,000g accelerometer
[28] Endevco https://www.endevco.com/
[29] Chen H, Shen S and Bao M 1996 Over-range capacity of a piezoresistive microaccelerometer *Sensors Actuators A* **58** 197
[30] Suminto J T 1996 A wide frequency range, rugged silicon micro accelerator with overrange stops *MEMS '96 Proc.* 180
[31] Dong J, Li X, Wang Y, Lu D and Ahat S 2002 Silicon micromachined high-shock accelerometers with a curved-surfaceapplication structure for over-range stop protection and free-mode-resonance depression *J. Micromech. Microeng.* **12** 742
[32] Yang Z and Li X 2006 Simulation and optimization on the squeeze-film damping of a novel high-g accelerometer *Microelectronics J.* **37** 383
[33] Thomson W 1856 On the electro-dynamic qualities of metals: Effects of magnetization on the electric conductivity of nickel and of iron *Proc. R. Soc. London.* **8** 546
[34] Butler R L and Dove R C 1966 The selection and evaluation of shock test instrumentation *Dynamics* 115
[35] Smith C S 1954 Piezoresistance effect in silicon and germanium *Phys. Rev.* **94** 42
[36] Matsuda K, Kanda Y, Yamamura K and Suzuki K 1990 Nonlinearity of piezoresistance effect in p-type and n-type silicon *Sensors Actuators A* **21** 45
[37] Matsuda K, Suzuki K, Yamamura K and Kanda Y 1993 Nonlinear piezoresistance effects of silicon *J. Appl. Phys.* **73** 1838
[38] Kanda Y 1982 A graphical representation of the piezoresistance coefficients in silicon *IEEE Trans. Electron Devices* **29** 64
[39] Kanda Y 1991 Piezoresistance effect of silicon *Sensors Actuators A* **28** 83
[40] Bridgman P W 1932 The effect of homogeneous mechanical stress on the electrical resistance of crystals *Phys. Rev.* **42** 858
[41] Liu J, Shi Y, Li P, Tang J, Zhao R and Zhang H 2012 Experimental study on the package of high-g accelerometer *Sensors Actuators A* **173** 1
[42] Qu X F and Su W 2002 High-g accelerometer in MEMS for penetrator weapon *Ordnance Industry Automation* **21** 7
[43] Huang S, Li X, Song Z, Wang Y, Yang H, Che L and Jiao J 2005 A high-performance micromachined piezoresistive accelerometer with axially stressed tiny beams *J. Micromech. Microeng.* **15** 993
[44] Shen S, Chen J and Bao M 1992 Analysis on twin-mass structure for a piezoresistive accelerometer *Sensors Actuators A* **34** 101
[45] Tsugai M and Bessho M 1987 Semiconductor accelerometer for automobile control *Tech. Digest, Int. Conf. on Solid-State Sensors and Actuators (Transducers 87)* 403
[46] Kanda Y and Yamamura K 1987 Silicon pressure sensors and accelerometer with four-terminal-gauge utilizing the shear stress *Tech. Digest, Int. Conf. on Solid-State Sensors and Actuators (Transducers 87)* 406
[47] Sandmaier H, Kühl K and Obermeier E 1987 A silicon based micromechanical accelerometer with cross acceleration sensitivity compensation *Tech. Digest, Int. Conf. on Solid-State Sensors and Actuators (Transducers 87)* 399
[48] Allen H W, Terry S C and DeBruin D W 1989 Accelerometer system with self-testable features *Sensors Actuators A* **20** 153
[49] Bao M 2000 *Micro Mechanical TransducersPressure Sensors, Accelerometers and Gyroscopes*

(Amsterdam: Elsevier)
[50] Burrer Chr, Esteve J, Plaza J A, Bao M 1994 Fabrication and characterization of a twin-mass accelerometer *Sensors Actuators A* **43** 115
[51] Chang D T, Kubena R L, Stratton F P, Kirby D J, Joyce R J and Kim J 2002 Wafer-bonded, high dynamic range, single-crystalline silicon tunneling acclerometer *Sensors. Proc. of IEEE* **2** 860
[52] Plößl A and Kräuter G 1999 Wafer direct bonding: tailoring adhesion between brittle materials *Materials Science and Engineering: R: Reports* **25** 1
[53] Partridge A, Reynolds J, Chui B, Chow E, Fitzgerald A, Zhang L, Maluf N and Kenny T 2000 A high performance planar piezoresistive accelerometer *J. Microelectromech. Syst.* **9** 58
[54] Brown T and Davis B 1998 Dynamic high-g loading of MEMS sensors: ground and flight testing *Proc. SPIE* **3512** 228
[55] Chen H, Shen S and Bao M 1997 Over-range capacity of a piezoresistive microaccelerometer *Sensors Actuators A* **58** 197
[56] Lee S W, Park S J, Kim J P, Lee S C and Cho D D 2000 Surface/bulk micromachined single-crystalline-silicon micro-gyroscope *J. Microelectromech. Syst.* **9** 557
[57] Park S J, Kwak D H, Ko H H, Song T Y and Cho D D 2005 Selective silicon-on-insulator (SOI) implant: A new micromachining method without footing and residual stress *J. Micromech. Microeng.* **15** 1607
[58] Lim M K, Du H, Su C and Jin W L 1999 A micromachined piezoresistive accelerometer with high sensitivity: design and modeling *Microelectronic Engineering* **49** 263
[59] Kuells R, Nau S, Salk M and Thoma K 2012 Novel piezoresistive high-g accelerometer geometry with very high sensitivity-bandwidth product *Sensors Actuators A* **182** 41
[60] Külls R, Nau S, Heß and Pilous N 2011 Development of a new MEMS High-g Accelerometer *NDIA 56th Annual Fuze Conf.*
[61] Wung T-S, Ning Y-T, Chang K-H, Tang S and Tsai Y-X 2014 Vertical-plate-type microaccelerometer with high linearity and low cross-axis sensitivity *Sensors Actuators A* In Press, Accepted Manuscript
[62] Zhang Z and Li K 2007 Design, simulation and multi-dimensional coupling research of monolithic MEMS three-axis high-g acclerometer *Proc. Int. Conf. on Information Acquisition* 280
[63] Shi J, Zhang W, Hao Y and Zeng Z 2004 Study to the integrated micro piezoresistive accelerometer for high g application with amplifying circuit *Proc. Int. Conf. on Solid-State and Integrated Circuits Technology* **3** 1820
[64] Kwon K and Park S 1998 A bulk-micromachined three-axis accelerometer using silicon direct bonding technology and polysilicon layer *Sensors Actuators A* **66** 250
[65] Lemkin M A, Boser B E, Auslander D and Smith J H A 1997 3-axis force balanced accelerometer using a single proof-mass *Tech. Digest, Int. Conf. Solid-State Sensors and Actuators (Transducers 97)* **2** 1185
[66] Bernard A and Touboul P 1990 Triaxial electrostatic accelerometer with dual electrical connection to its test weight *EP Patent* EP 0230198 B1
[67] Combi C O, Baldo L B, Faralli D M and Villa F F M 2008 Process for manufacturing a triaxial piezoresistive accelerometer and relative pressure-monitoring device *US Patent* US 7322236
[68] Mehregany M 2012 Three-axis accelerometers and fabrication methods *US Patent* US 8173470
[69] Ristic L, Calaway M F, Gutteridge R J, Dunn W C and Koucheng W 1995 Triaxial accelerometer *EP Patent* EP 0547742 B1
[70] Sooriakumar K S, Kok K W S and Patmon B K S 2008 Three-axis accelerometer *US Patent* US 7361523
[71] Yang X 2001 Three-axis accelerometer *WO Patent* WO 2001/075455 A2
[72] Zarabadi S and Christenson J 2007 Multiple-axis linear accelerometer *US Patent* US 7293460
[73] Dong P, Wu X Z and Li S Y 2007 A high-performance monolithic triaxial high-g accelerometer *Sensors. Proc. of IEEE* 768
[74] Rödjegård H, Johansson C, Enoksson P and Andersson G 2005 A monolithic three-axis SOI-

accelerometer with uniform sensitivity *Sensors Actuators A* **123** 50
[75] Matsumoto Y, Nishimura M, Matsuura M and Ishida M 1999 Three-axis SOI capacitive accelerometer with PLL C-V converter *Sensors Actuators A* **75** 77
[76] Wright N G and Horsfall A B 2007 SiC sensors: a review *J. Phys. D: Appl. Phys.* **40** 6345
[77] Atwell A R, Okojie R S, Kornegay K T, Roberson S L and Beliveau A 2003 Simulation, fabrication and testing of bulk micromachined 6H-SiC high-g piezoresistive accelerometers *Sensors Actuators A* **104** 11
[78] Okojie R S, Atwell A R, Kornegay K T, Roberson S L and Beliveau A 2002 Design considerations for bulk micromachined 6H-SiC high-g piezoresistive accelerometers *Tech. Digest, IEEE Int. Conf. on MEMS* 618
[79] Katulka G L, Hepner D J, Davis B, Irwin E, Ridgley M and Kornegay K T 2001 Characterization of silicon carbide and commercial-off-the-shelf (COTS) components for high-g launch and EM applications *IEEE Trans. on Magnetics* **37** 248
[80] Henisch H K and Roy R *Silicon Carbide* (New York: Pergamon Press)
[81] Hopcroft M A, Nix W D and Kenny T W 2010 What is the Young's Modulus of Silicon? *J. Microelectromech. Syst.* **19** 229
[82] Shor J S, Bemis L and Kurtz A D 1994 Characterization of monolithic n-type 6H-SiC piezoresistive sensing elements *IEEE Trans. Electron Devices* **41** 661
[83] Madou M J *The MEMS Handbook* (Boca Raton: CRC Press)
[84] PCB Piezotronics http://www.pcb.com/
[85] Gabrielson T B 1993 Mechanical-thermal noise in micromachined acoustic and vibration sensors *IEEE Trans. Electron Dev.* **40** 903
[86] Cleland A N and Roukes M L 2002 Noise processes in nanomechanical resonators *J. Appl. Phys.* **92** 2758
[87] Kaajakari V MEMS tutorial: Mechanical noise in microelectromechanical systems http://www.kaajakari.net/~ville/research/tutorials/tutorials.shtml
[88] Nyguist H 1928 Thermal agitation of electric charge in conductors *Phys. Rev.* **32** 110
[89] Endevco:Practical considerations of accelerometer noise *Endevco Technical Paper 324*
[90] Gautschi G *Piezoelectric Sensorics* (New York: Springer)
[91] Serridge M and Licht T R 1987 Piezoelectric accelerometer and vibration preamplifier handbook *(company publication)*. (Glostrup: Brüel & Kjær)
[92] Zutang W, Xianzhong S, Zhuangde J, Peng L, Lin G and Xingdong J 2005 A novel PVDF based high gn shock accelerometer *J. Phys. Conf. Series* **13** 107
[93] Curie J, Curie P 1880 Développement, par pression, de lélectricité polaire dans les cristaux hémièdres à faces inclinées *C. R. Acad. Sei.* **91** 294
[94] Yamaguchi K 1929 An accelerometer utilizing piezoelectricity *Bull. Inst. Phys. Chem. Research* **8** 157
[95] Kato Y and Nakamura S 1930 On the piezoelectric accelerometer and its use in the measurement of elastic waves produced by artificial shocks *Proc. Imp. Acad. (Tokyo)* **16** 272
[96] Tadigadapa S and Mateti K 2009 Piezoelectric MEMS sensors: state-of-the-art and perspectives *Meas. Sci. Technol.* **20** 1
[97] André B, Clot J, Partouche E and Simonne J J 1992 Thin film PVDF sensors applied to high acceleration measurements *Sensors Actuators A* **33** 111
[98] Benech P, Chambered E and Monllor C 1996 Acceleration measurement using PVDF *IEEE Trans. on Ultrasonics, Ferroelectrics and Frequency Control* **43** 838
[99] Daku B L F, Mohamed E M A and Prugger A F 2004 A PVDF transducer for low-frequency acceleration measurements *ISA Trans.* **43** 319
[100] Marat-Mendes R, Dias C J and Marat-Mendes J N 1999 Measurement of the angular acceleration using a PVDF and a piezo-composite *Sensors Actuators A* **76** 310
[101] Marcal R F M, Kovaleski J L and Suzim A A 1997 A poly vinylidene fluoride (PVF2) piezoelectric film based accelerometer *Proc. IEEE Instrumentation and Measurement Technology Conf., Sensing,*

Processing, Networking 908
[102] Spineanu A, Benabes P and Kielbasa R 1997 Digital piezoelectric accelerometer with sigma-delta servo technique *Sensors Actuators A* **60** 127
[103] Motamedi M E, Andrews A P and Brower E 1982 Accelerometer sensor using piezoelectric ZnO thin films *Proc. IEEE Ultrasonics Symp.* 303
[104] DeVoe D L and Pisano A P 2001 Surface micromachined piezoelectric accelerometers (PiXLs) *J. Microelectromech. Syst.* **10** 180
[105] Hui Y and Hang G 2007 Design of a bulk-micromachined piezoelectric accelerometer *Proc. IEEE Ultrasonics Symp.* 2598
[106] Zou Q, Tan W, Kim E S and Loeb G E 2008 Single- and triaxis piezoelectric-bimorph accelerometers *J. Microelectromech. Syst.* **17** 45
[107] Aoyagi S, Kumagai S, Yoshikawa D and Isono Y 2007 Surface micromachined accelerometer using ferroelectric substrate *Sensors Actuators A* **139** 88
[108] Beeby S P, Ross J N and White N M 2000 Design and fabrication of a micromachined silicon accelerometer with thick-film printed PZT sensors *J. Micromech. Microeng.* **10** 322
[109] Hindrichsen C C, Thomsen E V, Lou-Moller R and Bove T 2006 MEMS accelerometer with screen printed piezoelectric thick film *IEEE Conf. on Sensors* 1477
[110] Nemirovsky Y, Nemirovsky A, Muralt P and Setter N 1996 Design of novel thin-film piezoelectric accelerometer *Sensors Actuators A* **56** 239
[111] Wang L-P, Deng K, Zou L, Wolf R, Davis R J and Trolier-McKinstry S 2002 Microelectromechanical systems (MEMS) accelerometers using lead zirconate titanate thick films *IEEE Electron Device Lett.* **23** 182
[112] Wang L-P, Wolf R A, Wang Y, Deng K K, Zou L, Davis R J and Trolier-McKinstry S 2003 Design, fabrication, and measurement of high-sensitivity piezoelectric microelectromechanical systems accelerometers *J. Microelectromech. Syst.* **12** 433
[113] Yu H G, Zou L, Deng K, Wolf R, Tadigadapa S and Trolier-McKinstry S 2003 Lead zirconate titanate MEMS accelerometer using interdigitated electrodes *Sensors Actuators A* **107** 26
[114] Wang L-P, Ginsburg E, Gerfers F, Samara-Rubio D, Weinfeld B, Qing M, Rao V and He M Y 2006 Sputtered AlN thin films for piezoelectric MEMS devices *IEEE Conf. on Sensors* 10
[115] Gerfers F, Kohlstadt M, Bar H, He M-Y, Manoli Y and Wang L-P 2007 Sub-ug ultra-low-noise MEMS accelerometers based on CMOS-compatible piezoelectric AlN thin films *Tech. Digest, Int. Conf. Solid-State Sensors and Actuators (Transducers 07).* 1191
[116] Madou M J *Fundamentals of Microfabrication: The Science of Miniaturization* (Boca Raton: CRC Press)
[117] Trolier-McKinstry S and Muralt P 2004 Thin Film Piezoelectrics for MEMS *J. Electroceramics* **12** 7
[118] Baborowski J 2004 Microfabrication of piezoelectric MEMS *Int. Workshop on Smart Materials and Structures*
[119] Brüel & Kjær http://www.bksv.com/
[120] Kistler http://www.kistler.com/
[121] Pennington D 1965 Piezoelectric accelerometer manual *(company publication).* (Pasadena: Endevco)
[122] Choy S H, Wang X X, Chan H L W and Choy C L 2006 Study of compressive type accelerometer based on lead-free BNKBT piezoceramics *Appl. Phys. A* **82** 715
[123] Zhang S, Jiang X, Lapsley M, Moses P and Shrout T R 2010 Piezoelectric accelerometers for ultrahigh temperature application *Appl. Phys. Lett.* **96** 013506
[124] Bill B 1990 PiezoBEAM - ein neuartiges Konzept für Beschleunigungssensoren (PiezoBEAMAccelerometers: a proven and reliable design for modal analysis). *Messen & Prüfen* **3** 26
[125] Bill B and Wicks A L 1990 Measuring simultaneously translational and angular Acceleration with the new translational-angular piezobeam (TAP) system. *Sensors Actuators A* **21** 282